X-ray absorption and x-ray magnetic dichroism study on Ca_3CoRhO_6 and Ca_3FeRhO_6

T. Burnus,[1] Z. Hu,[1] Hua Wu,[1] J. C. Cezar,[2] S. Niitaka,[3,4] H. Takagi,[3,4,5] C. F. Chang,[1] N. B. Brookes,[2] H.-J. Lin,[6] L. Y. Jang,[6] A. Tanaka,[7] K. S. Liang,[6] C. T. Chen,[6] and L. H. Tjeng[1]

[1]*II. Physikalisches Institut, Universität zu Köln, Zülpicher Strasse 77, 50937 Köln, Germany*

[2]*European Synchrotron Radiation Facility, Boîte Postale 220, 38043 Grenoble, France*

[3]*Institute of Physical and Chemical Research, RIKEN, 2-1, Hirosawa, Wako, Saitama 351-0198, Japan*

[4]*CREST, Japan Science and Technology Agency (JST), Kawaguchi, Saitama 332-0012, Japan*

[5]*Department of Advanced Materials Science, University of Tokyo, 5-1-5, Kashiwanoha, Kashiwa, Chiba 277-8581, Japan*

[6]*National Synchrotron Radiation Research Center, 101 Hsin-Ann Road, Hsinchu 30077, Taiwan*

[7]*Department of Quantum Matter, ADSM, Hiroshima University, Higashi-Hiroshima 739-8530, Japan*

(Received 3 March 2008; revised manuscript received 9 April 2008; published 14 May 2008)

By using x-ray absorption spectroscopy at the Rh $L_{2,3}$, Co $L_{2,3}$, and Fe $L_{2,3}$ edges, we find a valence state of Co^{2+}/Rh^{4+} in Ca_3CoRhO_6 and of Fe^{3+}/Rh^{3+} in Ca_3FeRhO_6. X-ray magnetic circular dichroism spectroscopy at the Co $L_{2,3}$ edge of Ca_3CoRhO_6 reveals a giant orbital moment of about $1.7\mu_B$, which can be attributed to the occupation of the minority-spin d_0d_2 orbital state of the high-spin Co^{2+} ($3d^7$) ions in trigonal prismatic coordination. This active role of the spin-orbit coupling explains the strong magnetocrystalline anisotropy and Ising-type magnetism of Ca_3CoRhO_6.

DOI: 10.1103/PhysRevB.77.205111 PACS number(s): 78.70.Dm, 71.27.+a, 71.70.−d, 75.25.+z

I. INTRODUCTION

The quasi-one-dimensional (1D) transition-metal oxides Ca_3ABO_6 (A=Fe,Co,Ni, etc.; B=Co,Rh,Ir, etc.) have attracted a lot of interest in recent years because of their unique electronic and magnetic properties.[1–13] The structure of Ca_3ABO_6 contains 1D chains consisting of alternating face-sharing AO_6 trigonal prisms and BO_6 octahedra. Each chain is surrounded by six parallel neighboring chains forming a triangular lattice in the basal plane. Peculiar magnetic and electronic behaviors are expected to be related to geometric frustration in such a triangle lattice with antiferromagnetic (AFM) interchain interaction and Ising-type ferromagnetic (FM) intrachain coupling. $Ca_3Co_2O_6$, which realizes such a situation, shows stair-step jumps in the magnetization at regular intervals of the applied magnetic field of $M_s/3$, suggesting a ferrimagnetic spin alignment. It has a saturation magnetization of $M_s=4.8\mu_B$/f.u. at around 4 T.[14] Studies on the temperature and magnetic-field dependence of the characteristic spin-relaxation time suggest quantum tunneling of the magnetization similar to single-molecular magnets.[15] An applied magnetic field induces a large negative magnetoresistance, which is apparently not related to the three-dimensional magnetic ordering.[11] Band-structure calculations using the local-spin-density approximation plus Hubbard U (LSDA+U) predicted that the Co^{3+} ion at the trigonal site, which is in the high-spin (HS) state (S=2), has a giant orbital moment of $1.57\mu_B$ due to the occupation of the minority-spin d_2 orbital, while the Co^{3+} ion at the octahedral site is in the low-spin (LS) state (S=0).[16] An x-ray absorption and magnetic circular dichroism study at the Co $L_{2,3}$ edge has confirmed this prediction.[17] Both studies explain well the Ising nature of the magnetism of $Ca_3Co_2O_6$.

Ca_3CoRhO_6 and Ca_3FeRhO_6 have the same crystal structure as $Ca_3Co_2O_6$, but different magnetic and electronic properties: Neutron diffraction and magnetization measurements also indicated intrachain-FM and interchain-AFM interactions in Ca_3CoRhO_6 like in $Ca_3Co_2O_6$.[7] In contrast, the susceptibility data on Ca_3FeRhO_6 reveal a single transition into a three-dimensional AFM.[5,18] Although Ca_3CoRhO_6 has a similar magnetic structure as $Ca_3Co_2O_6$, it exhibits considerable differences in the characteristic temperatures in the magnetic susceptibility. The high-temperature limit of the magnetic susceptibility shows a Curie–Weiss behavior with a positive Weiss temperature of 150 K for Ca_3CoRhO_6,[5] while 30 K was found for $Ca_3Co_2O_6$.[2,3] The measured magnetic susceptibility undergoes two transitions at $T_{c_1}=90$ K and $T_{c_2}=25$ K for Ca_3CoRhO_6 and at $T_{c_1}=24$ K and $T_{c_2}=12$ K for $Ca_3Co_2O_6$,[3,5,7,8,12,18] which were attributed to FM-intrachain and AFM-interchain couplings, respectively. In contrast, Ca_3FeRhO_6 has an AFM ordering below $T_N=12$ K.[5,18,19] Unlike $Ca_3Co_2O_6$, there is only one plateau at 4 T and no saturation even at 18 T in the magnetization of Ca_3CoRhO_6 at 70 K.[7] A partially disordered state in Ca_3CoRhO_6 was inferred by the previous work of Niitaka *et al.*[8]

In order to understand the contrasting magnetic properties of Ca_3CoRhO_6 and Ca_3FeRhO_6 and, particularly, the type and origin of the intrachain magnetic coupling of these quasi-1D systems, the valence, spin, and orbital states have to be clarified. However, these issues have been contradictorily discussed in the previous theoretical and experimental studies. The general-gradient-approximated (GGA) density-functional band calculations[20] suggest a Co^{3+}/Rh^{3+} state in Ca_3CoRhO_6, while LSDA+U calculations with the inclusion of the spin-orbit coupling favor a Co^{2+}/Rh^{4+} state and, again, a giant orbital moment due to the occupation of minority-spin d_0 and d_2 orbitals.[21] Neutron diffraction experiments on Ca_3CoRhO_6 [8,22] suggest the Co^{3+}/Rh^{3+} state. However, based on the magnetic susceptibility[5] and x-ray photoemission spectroscopy,[23] the Co^{2+}/Rh^{4+} state was proposed. For Ca_3FeRhO_6, the Fe^{2+}/Rh^{4+} state was suggested in a magnetic susceptibility study,[5] whereas the Mössbauer spectroscopy indicates a Fe^{3+} state[19] and thus Rh^{3+}.

In order to settle the above issues, in this work, we first clarify the valence state of the Rh, Co, and Fe ions in Ca_3CoRhO_6 and Ca_3FeRhO_6 by using x-ray absorption spectroscopy (XAS) at the $L_{2,3}$ edges of Rh, Co, and Fe. We reveal a valence state of Co^{2+}/Rh^{4+} in Ca_3CoRhO_6 and of Fe^{3+}/Rh^{3+} in Ca_3FeRhO_6. Then, we investigate the orbital occupation and magnetic properties by using x-ray magnetic circular dichroism (XMCD) experiments at the Co $L_{2,3}$ edge of Ca_3CoRhO_6. We find a minority-spin d_0d_2 occupation for the HS Co^{2+} ground state and, thus, a giant orbital moment of about $1.7\mu_B$. As will be seen below, our results well account for the previous experiments.

II. EXPERIMENT

Polycrystalline samples were synthesized by a solid-state reaction and characterized by x-ray diffraction to be single phase.[5] The Rh $L_{2,3}$ XAS spectra were measured at the NSRRC 15B beamline in Taiwan, which is equipped with a double-Si(111) crystal monochromator for photon energies above 2 keV. The photon-energy resolution at the Rh $L_{2,3}$ edge ($h\nu \approx 3000-3150$ eV) was set to 0.6 eV. The Fe $L_{2,3}$ XAS spectrum of Ca_3FeRhO_6 was measured at the NSRRC Dragon beamline with a photon-energy resolution of 0.25 eV. The main peak at 709 eV of the Fe L_3 edge of single crystalline Fe_2O_3 was used for energy calibration. The Co $L_{2,3}$ XAS and XMCD spectra of Ca_3CoRhO_6 were recorded at the ID8 beamline of ESRF in Grenoble with a photon-energy resolution of 0.2 eV. The sharp peak at 777.8 eV of the Co L_3 edge of single crystalline CoO was used for energy calibration. The Co $L_{2,3}$ XMCD spectra were recorded in a magnetic field of 5.5 T; the photons were close to fully circularly polarized. The sample pellets were cleaved *in situ* in order to obtain a clean surface. The pressure was below 5×10^{-10} mbar during the measurements. All data were recorded in total-electron-yield mode. The Rh $L_{2,3}$ and Fe $L_{2,3}$ XAS spectra were measured at room temperature and the Co $L_{2,3}$ XAS and XMCD spectra at 50 K.

III. X-RAY ABSORPTION SPECTROSCOPY AND VALENCE STATE

We first concentrate on the valence of the rhodium ions in both studied compounds. For 4*d* transition-metal oxides, the XAS spectrum at the $L_{2,3}$ edge basically reflects the unoccupied t_{2g}- and e_g-related peaks in the O_h symmetry. This is due to the larger bandlike character and the stronger crystal-field interaction of the 4*d* states as well as due to the weaker intra-atomic interactions compared to 3*d* transition-metal oxides, where the intra-atomic multiplet interactions are dominant.[24,25] The intra-atomic multiplet and spin-orbit interactions in 4*d* elements only modify the relative intensity of the t_{2g}- and e_g-related peaks. Figure 1 shows the XAS spectra at the Rh $L_{2,3}$ edges of Ca_3FeRhO_6 (dashed line) and Ca_3CoRhO_6 (solid line). The Rh $L_{2,3}$ spectrum shows a simple, single-peaked structure at both Rh L_2 and Rh L_3 edges for Ca_3FeRhO_6, while an additional low-energy shoulder is observed for Ca_3CoRhO_6. Furthermore, the peak in the

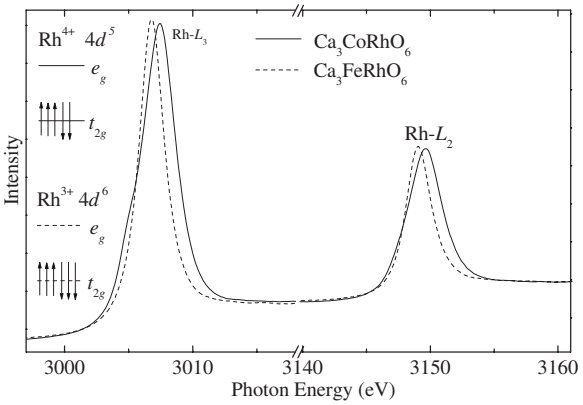

FIG. 1. The Rh $L_{2,3}$ XAS spectra of Ca_3CoRhO_6 and Ca_3FeRhO_6 and a schematic energy level diagram for Rh^{3+} $4d^6$ and Rh^{4+} $4d^5$ configurations in octahedral symmetry.

Ca_3CoRhO_6 spectrum is shifted by 0.8 eV to higher energies compared to that of the Ca_3FeRhO_6.

The single-peaked spectral structure for Ca_3FeRhO_6 indicates Rh^{3+} ($4d^6$) with completely filled t_{2g} orbitals, i.e., only transitions from the 2*p* core levels to the e_g states are possible. The results are in agreement with Mössbauer spectroscopy.[19] The shift to higher energies from Ca_3FeRhO_6 to Ca_3CoRhO_6 reflects the increase in the Rh valence from Rh^{3+} to Rh^{4+} as we can learn from previous studies on 4*d* transition-metal compounds.[24–27] Furthermore, for Ca_3CoRhO_6, the spectrum shows a weak low-energy shoulder, which is weaker at the Rh L_2 edge than at the Rh L_3 edge. This shoulder can be attributed to the transitions from the 2*p* core levels to the t_{2g} state, reflecting a $4d^5$ configuration with one hole at the t_{2g} state. Such spectral features were found earlier for Ru^{3+} in $Ru(NH_4)_3Cl_6$.[24,28] Detailed calculations reveal that the multiplet and spin-orbit interactions suppress the t_{2g}-related peak at the L_2 edge for a $4d^5$ configuration.[24–27] Thus, we find a Rh^{4+} ($4d^5$) state for Ca_3CoRhO_6. Having determined a Rh^{3+} state in Ca_3FeRhO_6 and a Rh^{4+} state in Ca_3CoRhO_6, we turn to the Fe $L_{2,3}$ and the Co $L_{2,3}$ XAS spectra to further confirm the Fe^{3+} state and the Co^{2+} state, as expected for charge balance.

Figure 2 shows the experimental Fe $L_{2,3}$ XAS spectra of Ca_3FeRhO_6 [Fig. 2(g)], along with those of [Fig. 2(a)] single crystalline Fe_2O_3 as an Fe^{3+} reference and of [Fig. 2(j)] FeO, which was taken from Ref. 29, as an Fe^{2+} reference. Additionally, the calculated spectra for different symmetries by using purely ionic (i.e., without Fe 3*d*–O 2*p* hybridization) crystal-field multiplet calculations[24,30,31] are shown. It is well known that an increase in the valence state of the 3*d* transition-metal ion by one causes a shift of the XAS $L_{2,3}$ spectra by about 1 eV toward higher energies.[32–34] The main peak of the Fe L_3 structure of the Ca_3FeRhO_6 lies 0.8 eV above the main peak of the divalent reference FeO and only slightly lower in energy than the one of Fe_2O_3 (Fe^{3+}). This indicates trivalent iron ions in Ca_3FeRhO_6. The slightly lower energy shift of Ca_3FeRhO_6 relative to Fe_2O_3 can be attributed to the weak trigonal crystal field in the former compared an octahedral field in the latter, as we will show below.

The experimental spectra of the reference compounds, Fig. 2(a) for Fe_2O_3 and Fig. 2(j) for FeO, can be well under-

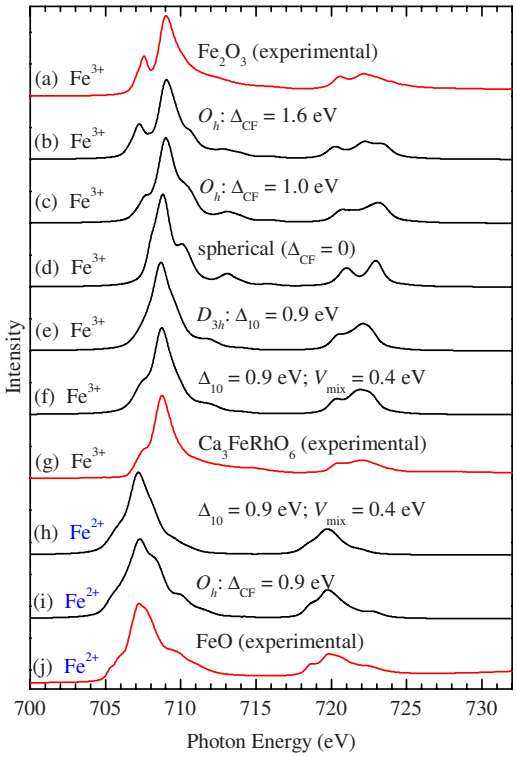

FIG. 2. (Color online) Experimental XAS spectra at the Fe $L_{2,3}$ edge of (a) Fe_2O_3 (Fe^{3+}), (g) Ca_3FeRhO_6, and (j) FeO (Fe^{2+}), which was taken from Park (Ref. 29), together with simulated [(b) and (c)] spectra in O_h, (d) spherical, and [(e) and (f)] D_{3h} symmetry for Fe^{3+} and simulated spectra in (h) D_{3h} and (i) O_h symmetry for Fe^{2+}. The simulated spectra have been broadend by a Gaussian with a HWHM of 0.2 eV and Lorentzian with a HWHM of 0.3 eV.

stood by using the multiplet calculations. For Fe_2O_3, we find a good simulation taking an Fe^{3+} ion in an octahedral symmetry with a t_{2g}-e_g splitting of 1.6 eV, which is depicted in Fig. 2(b). For FeO, a good match with the experiment can be found for the Fe^{2+} in an octahedral environment with a splitting of 0.9 eV [see curve Fig. 2(i)]. The weaker crystal field in FeO, compared to Fe_2O_3, is consistent due to its larger Fe-O bond length.

In order to understand the experimental Fe $L_{2,3}$ spectrum of Ca_3FeRhO_6, we first return to the Fe_2O_3 spectrum. When we reduce the t_{2g}-e_g splitting from 1.6 eV [Fig. 2(b)] via 1.0 eV [Fig. 2(c)] to 0.0 eV [Fig. 2(d)], we observe that the low-energy shoulder becomes washed out, while the high-energy shoulder becomes more pronounced.[30] Going further to a trigonal crystal field, the high-energy shoulder looses its intensity, as shown in curve Fig. 2(e) for a splitting of 0.9 eV between $d_{\pm 1}$ (d_{yz}/d_{zx}) and $d_0/d_{\pm 2}$ ($d_{3z^2-r^2}/d_{xy}/d_{x^2-y^2}$). The experimental Fe $L_{2,3}$ XAS spectrum of Ca_3FeRhO_6 in Fig. 2(g) can be well reproduced with this trigonal crystal field of 0.9 eV and in addition a mixing parameter V_{mix}=0.4 eV, which mixes the $d_{\pm 2}$ with the $d_{\mp 1}$ orbitals; the result for this Fe with the $3d^5$ high-spin configuration is presented in Fig. 2(f).

We note that Fig. 2(f) has been generated with the Fe in the trivalent state. As a check, we have also tried to fit the experimental spectrum of Ca_3FeRhO_6 by using a divalent Fe

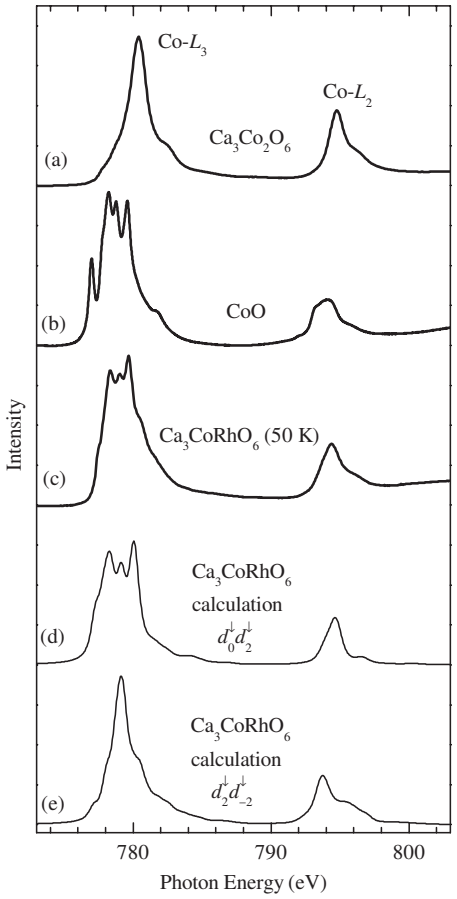

FIG. 3. The Co $L_{2,3}$ spectra of (a) $Ca_3Co_2O_6$ (Co^{3+}), (b) CoO (Co^{2+}), and (c) Ca_3CoRhO_6. The simulated spectra of high-spin Co^{2+} ($3d^7$) in trigonal prismatic symmetry are shown in (d) for d_0d_2 and in (e) for d_2d_{-2} minority-spin orbital occupations.

ansatz. However, the simulation does not match, as is illustrated in Fig. 2(h), in which we have used the same trigonal crystal field splitting of 0.9 eV and mixing parameter of 0.4 eV. To conclude, the Fe $L_{2,3}$ and Rh $L_{2,3}$ XAS spectra of Ca_3FeRhO_6 firmly establish the Fe^{3+}/Rh^{3+} scenario.

For the Ca_3CoRhO_6 system, the Rh $L_{2,3}$ XAS spectra suggest that the Rh ions are tetravalent, implying that the Co ions should be divalent. To confirm this Co^{2+}/Rh^{4+} scenario, we have to explicitly study the valence of the Co ion. Figure 3 shows the Co $L_{2,3}$ XAS spectra of Ca_3CoRhO_6 together with CoO as a Co^{2+} and $Ca_3Co_2O_6$ as a Co^{3+} reference.[17] Again, we see a shift to higher energies from CoO to $Ca_3Co_2O_6$ by about 1 eV. The Ca_3CoRhO_6 spectrum lies at the same energy position as the CoO spectrum confirming the Co^{2+}/Rh^{4+} scenario[21] and ruling out the Co^{3+}/Rh^{3+} scenario.[20] The result is fully consistent with the above finding from the Rh $L_{2,3}$ edge of Ca_3CoRhO_6 and in agreement with previous results from x-ray photoemission spectroscopy.[23]

IV. X-RAY MAGNETIC CIRCULAR DICHROISM AND ORBITAL OCCUPATION/MOMENT

After determining the valence states of Rh, Fe, and Co ions, we turn our attention to the orbital occupation and mag-

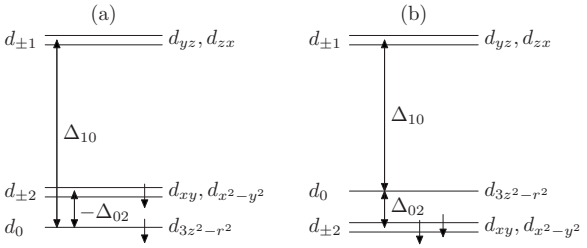

FIG. 4. Scheme of the two possible $3d$ occupations for a high-spin Co^{2+} ion in trigonal prismatic symmetry, ignoring the five up spins. (a) The d_0d_2 minority-spin occupation allows for a large orbital magnetic moment, whereas (b) for d_2d_{-2} the orbital moment vanishes.

netic properties of the Co^{2+} ion at the trigonal-prism site. This is motivated by the consideration that Co^{2+} ions may have a large orbital moment,[35] whose size depends on the details of the crystal field, while the high-spin Fe^{3+} ($3d^5$) and low-spin Rh^{3+} ($4d^6$) ions in Ca_3FeRhO_6 have a closed subshell without orbital degrees of freedom and thus no orbital moment.

In trigonal-prism symmetry, the $3d$ orbitals are split into $d_{\pm1}$, d_0, and $d_{\pm2}$ states (see Fig. 4). In terms of one-electron levels, the $d_{\pm1}$ orbitals lie highest in energy, while the lower lying d_0 and $d_{\pm2}$ usually are nearly degenerate. For a Co^{3+} d^6 system, it is *a priori* not obvious from band structure calculations to say which of these low lying orbitals gets occupied. Details, such as the inclusion of the spin-orbit interaction, can become crucial. Indeed, for $Ca_3Co_2O_6$, it was found from LDA+U calculations[16] and confirmed by XMCD measurements[17] that the spin-orbit interaction is crucial to stabilize the occupation of the d_2 orbital, thereby giving rise to giant orbital moments and Ising-type magnetism. For a Co^{2+} d^7 ion, however, the situation is quite different. As we will explain below, the double occupation of the d_0d_2 orbitals is energetically much more favored than that of the d_2d_{-2}: the energy difference could be of the order of 1 eV, while d_0 and $d_{\pm2}$ by themselves could be degenerate on a one-electron level. The consequences are straightforward: the double occupation of d_0d_2 [see Fig. 4(a)] should lead to a large orbital moment of $2\mu_B$ (neglecting covalent effects) and Ising type of magnetism with the magnetization direction fixed along the chains.[7,21] In contrast, the d_2d_{-2} [see Fig. 4(b)] would have given a quenched orbital moment.

In order to experimentally establish that the Co^{2+} ion has the d_0d_2 configuration, we have performed an XMCD study at the Co $L_{2,3}$ edges of Ca_3CoRhO_6. Figure 5 shows the Co $L_{2,3}$ XMCD spectrum of Ca_3CoRhO_6 taken at 50 K under 5.5 T. The spectra were taken, respectively, with the photon spin parallel (μ^+, red dotted curve) and antiparallel (μ^-, black solid curve) to the magnetic field. One can clearly observe large differences between the two spectra with the different alignments. Their difference, $\mu^+-\mu^-$, is the XMCD spectrum (blue dashed curve). An important feature of XMCD experiments is that there are sum rules, which were developed by Thole *et al.*[36] and Carra *et al.*,[37] to determine the ratio between the orbital ($m_{orb}=L_z$) and spin ($m_{spin}=2S_z$) contributions to the magnetic moment, namely,

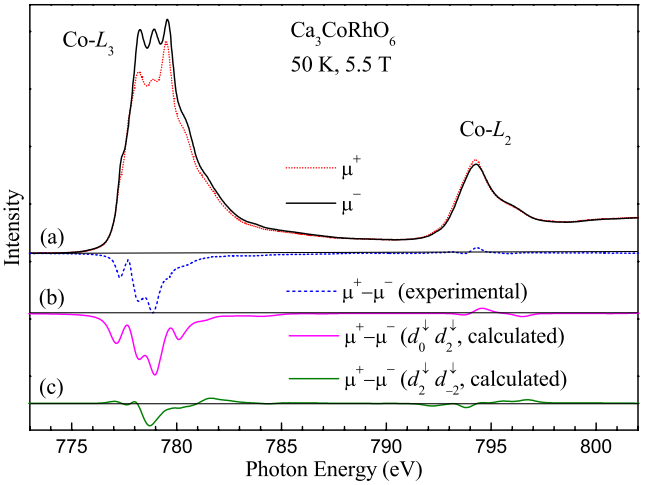

FIG. 5. (Color online) (a) Measured soft x-ray absorption spectra with parallel (μ^+, red dotted curve) and antiparallel (μ^-, black solid curve) alignment between photon spin and magnetic field, together with their difference (XMCD) spectrum ($\mu^+-\mu^-$, blue dashed curve); simulated XMCD spectra for (b) d_0d_2 (olive curve) and (c) d_2d_{-2} (magenta curve) minority-spin occupation of the high-spin Co^{2+}.

$$\frac{m_{orb}}{m_{spin}} = \frac{2}{3}\frac{\Delta L_3 + \Delta L_2}{\Delta L_3 - 2\Delta L_2}. \quad (1)$$

Here, ΔL_3 and ΔL_2 are the energy integrals of the L_3 and L_2 XMCD intensities. The advantage of these sum rules is that one needs not do any simulations of the spectra to obtain the desired quantum numbers. In our particular case, we can immediately recognize the presence of a large orbital moment in Fig. 5(a) since there is a large net (negative) integrated XMCD spectral weight. By using Eq. (1), we find $m_{orb}/m_{spin}=0.63$. Since the Co^{2+} ion is quite ionic, m_{spin} is very close to the expected ionic value of $3\mu_B$. For example, our LDA+U calculations yield $2.72\mu_B$ for the Co^{2+} ion ($2.64\mu_B$ for LDA) and Whangbo *et al.*[20] obtained $2.71\mu_B$ from GGA calculations. By using a value of $2.7\mu_B$ for the spin moment, we estimate $m_{orb}=1.7\mu_B$, which is in nice agreement with our LDA+U result of $1.69\mu_B$, for the d_0d_2 minority-spin orbital occupation.[21]

To critically check our experimental and previous LDA+U results[21] regarding the d_0d_2 orbital occupation and the giant orbital moment, we explicitly simulate the experimental XMCD spectra by using a charge-transfer configuration-interaction cluster calculation,[38,39] which includes not only the full atomic multiplet theory and the local effects of the solid but also the O $2p$–Co $3d$ hybridization. The results of the calculated Co $L_{2,3}$ XAS and XMCD spectra are presented in Figs. 3(d) and 5(b), respectively. We can clearly observe that the simulations reproduce the experimental spectra very well. The parameters[40] used are those which indeed give the d_0d_2 orbital occupation for the ground state. The magnetic quantum numbers found are $m_{orb}=1.65\mu_B$ and $m_{spin}=2.46\mu_B$, yielding $m_{orb}/m_{spin}=0.67$ and a total Co magnetic moment of $4.11\mu_B$. With the Rh in the $S=1/2$ tetravalent state, the total magnetic moment per formula unit should be around $5\mu_B$. This is not inconsistent with the results of the

high-field magnetization study by Niitaka *et al.*:[7] they found a total moment of $4.05\mu_B$, but there the saturation of the magnetization has not yet been reached even under 18.7 T. This can now be understood since the magnetocrystalline anisotropy, which is associated with the active spin-orbit coupling, is extremely strong and makes it difficult to fully magnetize a powder sample as was used in their study.

We also have simulated the spectra for the d_2d_{-2} scenario. These are depicted in Fig. 3(e) for the XAS and in Fig. 5(c) for the XMCD. It is obvious that the experimental spectra are not reproduced. The simulated line shapes are very different from the experimental ones and the integral of the simulated XMCD spectrum yields a vanishing orbital moment. We therefore can safely conclude that the ground state of this material is not d_2d_{-2}. For completeness, we mention that the magnetic quantum numbers found for this d_2d_{-2} ansatz are $m_{\mathrm{orb}}=0.20\mu_B$ and $m_{\mathrm{spin}}=2.86\mu_B$, yielding $m_{\mathrm{orb}}/m_{\mathrm{spin}}=0.07$ and a total Co magnetic moment of $3.06\mu_B$.

V. STABILITY OF THE d_0d_2 STATE

Having established that the ground state of Ca_3CoRhO_6 has the Co^{2+} d^7 ion in the doubly occupied d_0d_2 orbital configuration and not in the d_2d_{-2}, it is interesting to study its stability in more detail. As already mentioned above, for a Co^{3+} d^6 ion, the d_0 and $d_{\pm2}$ states can be energetically very close to each other. For a Co^{2+} d^7 ion, however, the d_0d_2 and d_2d_{-2} states are very much different in energy. This is illustrated in the top panel of Fig. 6, in which we have calculated the occupation numbers of the d_0, d_2, and d_{-2} orbitals as a function of Δ_{02}, the one-electron level splitting between the d_0 and $d_{\pm2}$ orbitals. The d_0d_2 ground state, which gives the best simulation to the experimental XAS and XMCD spectra, was obtained with $\Delta_{02}\approx0.4$ eV. We can observe that the d_0d_2 situation is quite stable for a wide range of Δ_{02} values, certainly up to 0.8 eV. With a transition region between $\Delta_{02}=0.8-1.2$ eV, we find a stable d_2d_{-2} situation only for Δ_{02} values larger than 1.2 eV. (For the d_2d_{-2} simulations above, we have used $\Delta_{02}=1.4$ eV.) This is a very large number indeed, and it can be traced back to the multiplet character of the on-site Coulomb interactions: an occupation of d_2d_{-2} means a much stronger overlap of the electron clouds compared to the case for a d_0d_2. This results in a higher repulsion energy, which is not a small quantity in view of the atomiclike values of the F^2 and F^4 Slater integrals determining the multiplet splitting.[38,41]

In the middle panel of Fig. 6, we also show the expectation values for m_{orb} and m_{spin} when varying Δ_{02}. Again, we clearly observe that the large orbital-moment situation is quite stable. To quench the orbital moment, one would need much higher Δ_{02} values. Important is that the spin state does not change here. The bottom panel of Fig. 6 demonstrates that the high-spin state of the Co^{2+} ion is not affected by Δ_{02}: the expectation value $\langle S^2\rangle$ remains constant throughout at a value consistent with an essentially $S=3/2$ state. Obviously, the L^2 and J^2 quantum numbers are strongly affected by Δ_{02}.

VI. CONCLUSION

To summarize, the Rh $L_{2,3}$, Co $L_{2,3}$, and Fe $L_{2,3}$ XAS measurements indicate Co^{2+}/Rh^{+} in Ca_3CoRhO_6 and

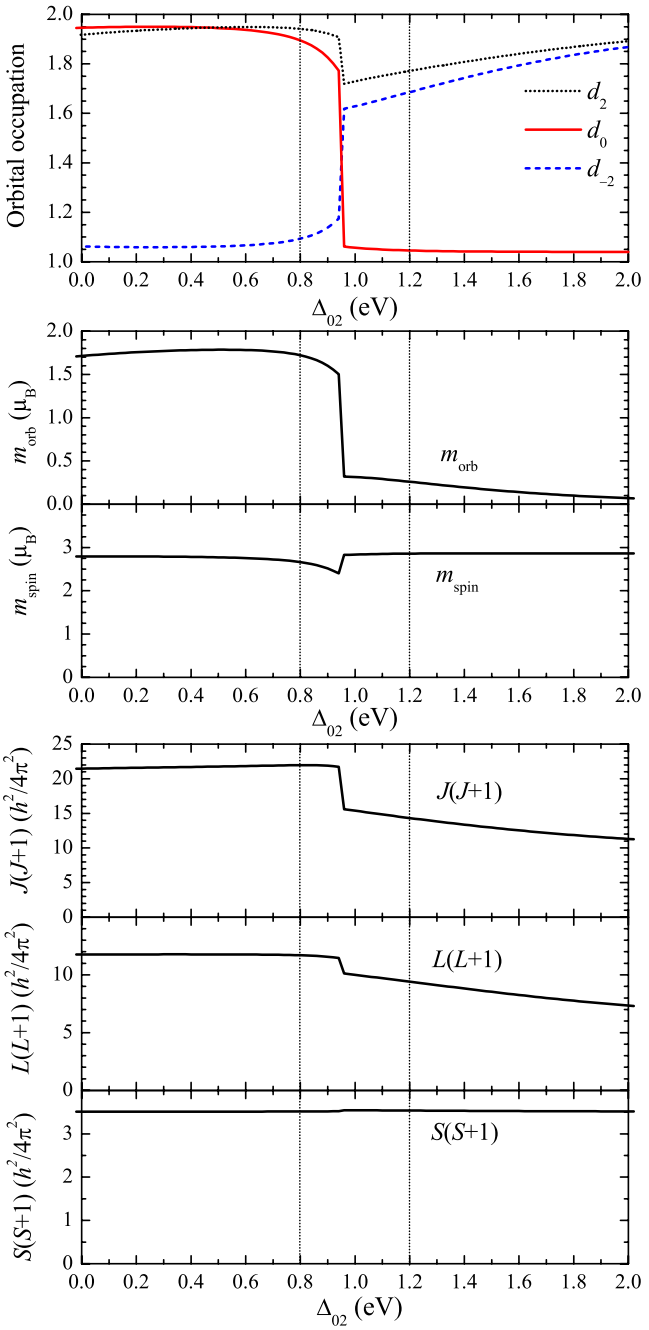

FIG. 6. (Color online) Top panel: Occupation number of the d_0, d_2, and d_{-2} orbitals as a function of the d_0-$d_{\pm2}$ splitting Δ_{02} [Fig. 4(b)]. Middle panel: Orbital and spin moments (m_{orb} and m_{spin}) as function of Δ_{02}. Bottom panel: $J(J+1)$, $L(L+1)$, and $S(S+1)$ as a function of Δ_{02}.

Fe^{3+}/Rh^{3+} in Ca_3FeRhO_6. The magnetic properties of Ca_3FeRhO_6 are relatively simple as both the HS Fe^{3+} and LS Rh^{3+} ions have a closed subshell and thus no orbital degrees of freedom and no orbital moment. The weak intrachain AFM coupling between the HS Fe ions can be understood in terms of the normal superexchange via the intermediate nonmagnetic O-Rh-O complex. For Ca_3CoRhO_6, the combined experimental and theoretical study of the Co $L_{2,3}$ XAS and XMCD spectra reveals a giant orbital moment of about $1.7\mu_B$. This large orbital moment is connected with the

minority-spin d_0d_2 occupation for HS Co^{2+} ($3d^7$) ions in the peculiar trigonal prismatic coordination. The high FM ordering temperature in Ca_3CoRhO_6, compared to that of $Ca_3Co_2O_6$, can be attributed to the distinct octahedral sites (which mediate the Co-Co magnetic coupling): the magnetic Rh^{4+} ion ($S=1/2$) in the former and the nonmagnetic Co^{3+} ion ($S=0$) in the latter.

ACKNOWLEDGMENTS

We would like to thank Lucie Hamdan for her skillful technical and organizational assistance in preparing the experiment. The research in Köln is supported by the Deutsche Forschungsgemeinschaft through SFB 608.

[1] H. Fjellvåg, E. Gulbrandsen, S. Aasland, A. Olsen, and B. C. Hauback, J. Solid State Chem. **124**, 190 (1996).
[2] S. Aasland, H. Fjellvåg, and B. Hauback, Solid State Commun. **101**, 187 (1997).
[3] H. Kageyama, K. Yoshimura, K. Kosuge, H. Mitamura, and T. Goto, J. Phys. Soc. Jpn. **66**, 1607 (1997).
[4] H. Kageyama, K. Yoshimura, K. Kosuge, M. Azuma, M. Takano, H. Mitamura, and T. Goto, J. Phys. Soc. Jpn. **66**, 3996 (1997).
[5] S. Niitaka, H. Kageyama, M. Kato, K. Yoshimura, and K. Kosuge, J. Solid State Chem. **146**, 137 (1999).
[6] A. Maignan, C. Michel, A. C. Masset, C. Martin, and B. Raveau, Eur. Phys. J. B **15**, 657 (2000).
[7] S. Niitaka, H. Kageyama, K. Yoshimura, K. Kosuge, S. Kawano, N. Aso, A. Mitsuda, H. Mitamura, and T. Goto, J. Phys. Soc. Jpn. **70**, 1222 (2001).
[8] S. Niitaka, K. Yoshimura, K. Kosuge, M. Nishi, and K. Kakurai, Phys. Rev. Lett. **87**, 177202 (2001).
[9] B. Martínez, V. Laukhin, M. Hernando, J. Fontcuberta, M. Parras, and J. M. González-Calbet, Phys. Rev. B **64**, 012417 (2001).
[10] E. V. Sampathkumaran and A. Niazi, Phys. Rev. B **65**, 180401(R) (2002).
[11] B. Raquet, M. N. Baibich, J. M. Broto, H. Rakoto, S. Lambert, and A. Maignan, Phys. Rev. B **65**, 104442 (2002).
[12] V. Hardy, M. R. Lees, A. Maignan, S. Hébert, D. Flahaut, C. Martin, and D. Mc K. Paul, J. Phys.: Condens. Matter **15**, 5737 (2003).
[13] X. Yao, S. Dong, K. Xia, P. Li, and J.-M. Liu, Phys. Rev. B **76**, 024435 (2007).
[14] A. Maignan, V. Hardy, S. Hébert, M. Drillon, M. R. Lees, O. Petrenko, D. Mc K. Paul, and D. Khomskii, J. Mater. Chem. **14**, 1231 (2004).
[15] V. Hardy, D. Flahaut, M. R. Lees, and O. A. Petrenko, Phys. Rev. B **70**, 214439 (2004).
[16] H. Wu, M. W. Haverkort, Z. Hu, D. I. Khomskii, and L. H. Tjeng, Phys. Rev. Lett. **95**, 186401 (2005).
[17] T. Burnus, Z. Hu, M. W. Haverkort, J. C. Cezar, D. Flahaut, V. Hardy, A. Maignan, N. B. Brookes, A. Tanaka, H. H. Hsieh, H.-J. Lin, C.-T. Chen, and L. H. Tjeng, Phys. Rev. B **74**, 245111 (2006).
[18] M. J. Davis, M. D. Smith, and H.-C. zur Loye, J. Solid State Chem. **173**, 122 (2003).
[19] S. Niitaka, K. Yoshimura, K. Kosuge, K. Mibu, H. Mitamura, and T. Goto, J. Magn. Magn. Mater. **260**, 48 (2003).
[20] M.-H. Whangbo, D. Dai, H.-J. Koo, and S. Jobic, Solid State Commun. **125**, 413 (2003).
[21] H. Wu, Z. Hu, D. I. Khomskii, and L. H. Tjeng, Phys. Rev. B **75**, 245118 (2007).
[22] M. Loewenhaupt, W. Schäfer, A. Niazi, and E. V. Sampathkumaran, Europhys. Lett. **63**, 374 (2003).
[23] K. Takubo, T. Mizokawa, S. Hirata, J.-Y. Son, A. Fujimori, D. Topwal, D. D. Sarma, S. Rayaprol, and E. V. Sampathkumaran, Phys. Rev. B **71**, 073406 (2005).
[24] F. M. F. de Groot, Z. W. Hu, M. F. Lopez, G. Kaindl, F. Guillot, and M. Tronc, J. Chem. Phys. **101**, 6570 (1994).
[25] Z. Hu, H. von Lips, M. S. Golden, J. Fink, G. Kaindl, F. M. F. de Groot, S. Ebbinghaus, and A. Reller, Phys. Rev. B **61**, 5262 (2000).
[26] Z. Hu, M. S. Golden, S. G. Ebbinghaus, M. Knupfer, J. Fink, F. M. F. de Groot, and G. Kaindl, Chem. Phys. **282**, 451 (2002).
[27] R. K. Sahu, Z. Hu, M. L. Rao, S. S. Manoharan, T. Schmidt, B. Richter, M. Knupfer, M. Golden, J. Fink, and C. M. Schneider, Phys. Rev. B **66**, 144415 (2002).
[28] T. K. Sham, J. Am. Chem. Soc. **105**, 2269 (1983).
[29] J.-H. Park, Ph.D. thesis, University of Michigan, 1994.
[30] F. M. F. de Groot, J. C. Fuggle, B. T. Thole, and G. A. Sawatzky, Phys. Rev. B **42**, 5459 (1990).
[31] See Theo Thole Memorial Issue, J. Electron Spectrosc. Relat. Phenom. **86**, 1 (1997).
[32] C. T. Chen and F. Sette, Phys. Scr., T **T31**, 119 (1990).
[33] C. Mitra, Z. Hu, P. Raychaudhuri, S. Wirth, S. I. Csiszar, H. H. Hsieh, H.-J. Lin, C. T. Chen, and L. H. Tjeng, Phys. Rev. B **67**, 092404 (2003).
[34] T. Burnus, Z. Hu, H. H. Hsieh, V. L. J. Joly, P. A. Joy, M. W. Haverkort, H. Wu, A. Tanaka, H.-J. Lin, C. T. Chen, and L. H. Tjeng, Phys. Rev. B **77**, 125124 (2008).
[35] G. Ghiringhelli, L. H. Tjeng, A. Tanaka, O. Tjernberg, T. Mizokawa, J. L. de Boer, and N. B. Brookes, Phys. Rev. B **66**, 075101 (2002).
[36] B. T. Thole, P. Carra, F. Sette, and G. van der Laan, Phys. Rev. Lett. **68**, 1943 (1992).
[37] P. Carra, B. T. Thole, M. Altarelli, and X. Wang, Phys. Rev. Lett. **70**, 694 (1993).
[38] A. Tanaka and T. Jo, J. Phys. Soc. Jpn. **63**, 2788 (1994).
[39] J. Okamoto, K. Mamiya, S.-I. Fujimori, T. Okane, Y. Saitoh, Y. Muramatsu, K. Yoshii, A. Fujimori, A. Tanaka, M. Abbate, T. Koide, S. Ishiwata, S. Kawasaki, and M. Takano, Phys. Rev. B **71**, 104401 (2005).
[40] Parameters (in eV): $U_{3d,3d}=5$, $U_{2p,3d}=6.5$, $\Delta=4$, $\Delta_{10}^{\text{ionic}}=0.65$, $V_{\text{mix}}^{\text{ionic}}=-0.2$, $V_{pd\sigma}=-1.024$, $H_{\text{ex}}=0.045$. The Slater integrals were reduced to 80% of their Hartree-Fock value. $\Delta_{02}^{\text{ionic}}=0.4$ (d_0d_2 scenario): $\Delta_{02}^{\text{ionic}}=1.4$ (d_2d_{-2}). The simulated spectra have been broadend by a Gaussian with a half-width at half maximum (HWHM) of 0.2 eV and Lorentzian with a HWHM of 0.2 eV.
[41] E. Antonides, E. C. Janse, and G. A. Sawatzky, Phys. Rev. B **15**, 1669 (1977).